Applied Physics Letters

On-chip beam positioning sensor via frequency locked cascaded ring resonators

Cite as: Appl. Phys. Lett. **112**, 201112 (2018); https://doi.org/10.1063/1.5029999
Submitted: 18 March 2018 . Accepted: 04 May 2018 . Published Online: 18 May 2018

Alex Naiman, Liron Stern, and Uriel Levy

On-chip beam positioning sensor via frequency locked cascaded ring resonators

Alex Naiman, Liron Stern, and Uriel Levy
Department of Applied Physics, The Benin School of Engineering and Computer Science, The Center for Nanoscience and Nanotechnology, The Hebrew University of Jerusalem, Jerusalem 91904, Israel

(Received 18 March 2018; accepted 4 May 2018; published online 18 May 2018)

We demonstrate an approach for on-chip beam positioning with a position accuracy of up to 100 nm. This approach is based on tracking the resonance of two adjacent microring resonators that are implemented on a silicon on insulator chip. We demonstrate the functionality of our approach by illuminating the chip through a Near Field Scanning Optical Microscope tip and monitoring the shift of the microring resonances due to the thermo-optic effect. We also discuss the contribution of different effects such as free carrier absorption and dispersion to the resonance shift. *Published by AIP Publishing*. https://doi.org/10.1063/1.5029999

Devices for high accuracy beam positioning and alignment are in great demand for a myriad of applications including atomic force microscopy[1] (AFM), spatial imaging with optical tweezers,[2,3] and target acquisition,[4] to name a few. Beam positioning is typically mitigated by the use of commercially available position sensitive detectors (PSDs), e.g., segmented PSDs or lateral effect PSDs. Segmented PSDs are common substrate photodiodes divided into two (in the 1D configuration) or four (in the 2D configuration) segments, separated by a gap. The position can be deduced from the difference in voltage between the photodiode segments. Typical accuracy for such PSDs is on the order of few micrometers[5] depending on the light intensity and beam radius. Clearly, the beam radius needs to be sufficiently large to cover all photodiode segments; otherwise, differential measurements cannot be achieved. For commercial devices, the gap between the segments is about 50 μm, and so, beams with a radius over 100 μm are typically desired. The second type of commonly used device is the lateral effect PSD,[6] which is based on the lateral photoeffect to perform differential measurements and determine the beam position. For this family of devices, there is no lower limit on the beam radius and the accuracy is high, around 1 μm. On the other hand, such devices suffer from non-linearity[7] due to non-uniform surface resistance which reduces their precision and reliability.

Hereby, we propose and experimentally demonstrate an attractive alternative implementation of beam positioning devices based on the realization of microring resonators on a chip. On-chip micro ring resonators (MRRs) are now well established and are used in variety of applications, e.g., label free bio-sensing, waveform generation,[8,9] electro-optical modulation,[10,11] thermal sensing,[12,13] and more. MRRs can be fabricated with relative ease, and among many other advantages, the combination of chip scale integration[14] and the shift of the resonance frequency with respect to the refractive index of an external environment allows the correlation between chip scale spectroscopic measurements and variations in the refractive index. Our approach takes advantage of this property. It relies on a scheme consisting of two cascaded MRRs that are coupled to the same bus waveguide (WG). The two MRRs are designed to be identical in their dimensions and consequently their resonant frequencies. However, due to unavoidable fluctuations in the fabrication process, the resonance wavelengths of the two MRRs with a Q factor of 6×10^4 are shifted by a few GHz ($\sim$40 pm) from one another as can be seen in the supplementary material. Taking advantage of that, we can precisely measure the shift in resonance of one MRR with respect to the other upon light illumination. Owing to the fact that the two resonators are in close proximity to each other (separated by only 15 μm), our device operates in a common mode rejection, i.e., it provides an excellent reference allowing us to eliminate global effects such as environmental fluctuations in temperature and humidity. Furthermore, it allows us to perform highly accurate measurements of the beat frequency between the two resonances in the radio frequency (RF) domain, as was recently demonstrated in Ref. 15.

Our device is constructed on a silicon on insulator (SOI) chip consisting of a 220 nm thick silicon device layer on top of 2 μm buried oxide. Standard UV lithography was used for patterning of the 450 nm wide bus WG and the two MRRs which are 15 μm in radius and are separated by 15 μm from each other. The waveguides are etched to a thickness of about 70 nm, thus having a rib thickness of $\sim$150 nm. The structure is covered by a 1 μm thick PECVD silicon dioxide layer, serving as the upper cladding. The experimental scheme can be seen in Fig. 1. Two tunable near infrared (IR, Agilent 81680A) lasers are coupled to the bus WG via a lensed fiber, and each laser is aligned to a resonance of one of the MRRs. Light is collected by a photodetector feeding a feedback loop and by another fast photo-detector to measure the beat frequency between the lasers. The lasers and the photodetector are connected to a feedback loop, as previously reported[15] which locks each of the lasers to their corresponding MRR resonance.

Next, we introduce a 635 nm light source through an aperture of an NSOM tip which is positioned over the MRRs as illustrated in Fig. 2. The optical power emerging out of the tip was measured to be in the few μW range, and the spot radius is about 1 μm. Given the significant absorption of light by the silicon layer at this wavelength ($\alpha = 1.9 \times 10^3$ cm^{-1}),

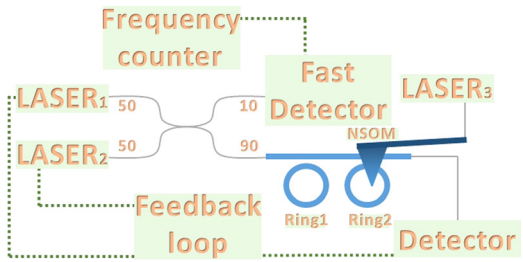

FIG. 1. The experimental scheme, where $Laser_1$ and $Laser_2$ are the tunable near infrared (IR) lasers which are combined to a polarization maintaining fiber via a 50/50 coupler. The fiber is then split into two branches 10/90 where the 10% falls on the fast photodetector which is connected to the frequency counter for beating frequency measurements. The remaining 90% are coupled via lensed fiber to the silicon chip with the microring resonators (MRRs) and collected by a photodetector at the waveguide (WG) output. The signal from the photodetector is then used for the feedback loop. $Laser_3$ is a $\lambda = 635$ nm diode laser coupled to a Near Field Scanning Optical Microscope (NSOM) tip positioned over the MRRs on the silicon chip.

some of the incident light gives rise to the photogeneration of free carriers, which in turn results in free carrier absorption, free carrier dispersion, and localized heating. In order to determine the contribution of the different effects to the change in the refractive index of the silicon, we have first estimated the photo-generation rate in the SOI slab to be $= 3 \times 10^{24}\,\mathrm{cm^{-3}s^{-1}}$. In order to obtain the excess carrier density due to the photo-generation, we need to multiply the generation rate by the lifetime of the free carriers[16,17] which is around 1 ns for SOI. The excess free carriers due to the photo-generation result in

$$\delta n = \delta p = \tau \times G = 3 \times 10^{15}\,\mathrm{cm^{-3}}. \tag{1}$$

The effect of these excess carriers on the refractive index of silicon can be estimated using empirical Soref's & Bennett's equation[18]

$$\Delta n = -\left[8.8 \times 10^{-22} \times \delta n + 8.5 \times 10^{-18} \times (\delta p)^{0.8}\right] = -2.3 \times 10^{-5}. \tag{2}$$

While such a refractive index change is not negligible, its effect is localized, as the refractive index decays to e^{-1} at a distance of around a micron. Thus, the resonance shift due to free carrier plasma dispersion is negligible. For the same reason, free carrier absorption can be neglected.

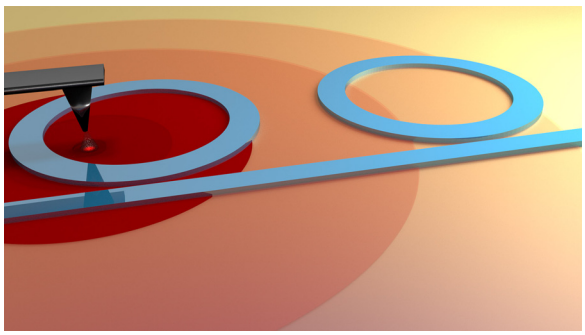

FIG. 2. Schematic representation of the cascaded MRRs and NSOM scheme, including color representation of the temperature distribution profile generated by the light sources coupled to the NSOM probe.

We now deal with the more significant effect, namely, the influence of the thermo-optic effect on the resonance frequency. This can be done by solving the heat equation in the presence of the localized heat source in the form of light absorption. Doing so (not shown here), we find a refractive index change of $\Delta n = 10^{-6}$. At a first glance, it seems that the thermo-optics effect is milder than the free carrier dispersion effect. Yet, one should bear in mind that the temperature distribution is significantly broader, as the temperature decays logarithmically with the distance. In fact, we have noticed that the accumulative effect as a result of heating is significantly more dominant as compared to the free carrier effect. We thus assume that our experimental results are mostly driven by thermal effects. During the experiment, the tip was in contact with the oxide cladding and moved in constant intervals along the line connecting the centers of the two MRRs as denoted by the orange dashed line in Fig. 4. At each position of the tip, the beating frequency between the two resonances (Δf_{off}) was measured twice, first with the laser turned off, followed by turning the laser on and measuring the beating frequency again (Δf_{on}). The change in the beating frequency is denoted as $\Delta f = \Delta f_{on}$-Δf_{off}, and it corresponds to the temperature induced refractive index gradient between the two MRRs. The relation between frequencies as the refractive index change is given by $\Delta f/f = \Delta n/n_g$, where f is the laser frequency which is locked to the resonance frequency of the MRR. The locking scheme operates at a telecom wavelength of $\lambda = 1.5$ μm, n_g is the group index of the silicon waveguide, calculated to be 3.8, and $\Delta n = \Delta n_2$-Δn_1, where $\Delta n_{1,2}$ is the change in the effective refractive index of MRR 1 or 2 due to the local heating induced by the light emitted from the NSOM tip. Taking into account the thermo-optic coefficient of silicon (1.8×10^{-4}) and the confinement factor of the mode, we can extract the temperature difference between the two MRRs, which varies from few milli-Kelvins to tens of milli-Kelvins, corresponding to the cases where the tip is positioned far away from the MRRs and where the tip is positioned in close proximity and even directly above one of the MRRs. The correlation of Δf to the position of the illumination is shown schematically in Fig. 3, where three different positions of illumination are considered alongside their effect on the frequency difference Δf. Figure 3(a) demonstrates the case where the illumination is off, and the beating frequency is Δf_{off}. Figure 3(b) demonstrates the MRRs spectrum for the case where the illumination is on top of MRR1, in such a case $\Delta f_{off} > \Delta f_{on}$ and a negative frequency difference is measured ($\Delta f < 0$). Finally, Fig. 3(c) demonstrates a case where the illumination is mostly over MRR2, and therefore, $\Delta f_{off} < \Delta f_{on}$ and the frequency difference is positive ($\Delta f > 0$).

Once the working principle is made clear, we turn to Fig. 4. to present the measured frequency shift (purple circles) along with the simulated frequency shift (solid blue line). The simulation is based on a finite element electromagnetic module of COMSOL multiphysics for calculating the spot size of the $\lambda = 635$ nm diode laser beam emitted out of the NSOM tip and its absorption within the silicon rib. This simulation result has been used as the heat source for a thermal simulation to determine the on-chip temperature distribution due to the local heating by the absorbed light, by

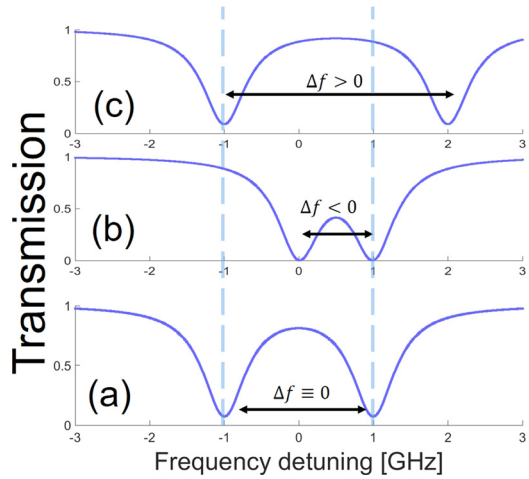

FIG. 3. (a)–(c) Schematic representation of the Resonance shift due to heating by the light emitted from the NSOM tip for three cases: (a) When there is no light emission, (b) The light source is over the left MRR (MRR1), and (c) The light source is over the right MRR (MRR2).

solving the time independent heat equation. Once the temperature profile was obtained, it was translated to the refractive index change by the use of the thermo-optic coefficient of silicon (1.8×10^{-4}), taking into account the confinement factor of the optical waveguide mode. Having the refractive index variations in hand, one can calculate the accumulated phase change and the resonance frequency change which is different for each MRR depending on the distance from the center of the temperature gradient, which is logarithmic for this configuration. Looking carefully at Fig. 4, one can observe the experimental data and the simulation results, with reasonably good agreement between the two. We can divide the graph into 3 regions: (1) The region between the MRRs where the slope is the steepest due to the maximal temperature difference in this region as temperature decays logarithmically (green region). (2) The region within the MRR which shows a more moderate slope. This is because within a MRR the generated heat, and correspondingly, the accumulated phase is not dependent on the location of the heat spot. (3) The region outside the MRRs where the signal decays logarithmically due to the logarithmic profile of the temperature distribution (blue region). As one can see there are some discrepancies between the simulation and the experimental results in this region. Such a discrepancy can probably be resolved with a more accurate heat dissipation model which takes heat convection and radiation into account.

Furthermore, in the transition between the regions, we can see discontinuities which occur due to the free carrier effect which is more local in nature. Furthermore, one can observe the change in frequency as a function of NSOM probe position. This value obtains its minimum (or maximum in negative units) when the tip is positioned on top of the left MRR. Similarly, the maximal value is obtained when the tip is positioned over the right MRR. Between the MRRs, there is a point where both MRRs reach the same temperature and no frequency shift can be witnessed. This symmetry point is very subtle, and an accurate positioning of the illumination spot can be achieved with an accuracy of ± 100 nm for long data acquisition times of about 100 s. A lower accuracy of $\pm 1\,\mu$m is obtained for short acquisition times of about 1 s. The accuracy is estimated based on the Allan deviation measurement as shown in the supplementary material.

In conclusion, we have demonstrated a scheme which allows the accurate positioning of a laser beam of light using an on-chip differential optical resonator system. We showed that for the configuration used in our experiment, the main contribution to the refractive index change is the thermo-optic effect. An accuracy of about $\pm 1\,\mu$m is obtained for short integration times in the range of a second. The positioning accuracy can be as low as ± 100 nm for longer integration times, in the range of 100 s. We have also performed simulations for different input powers and different beam

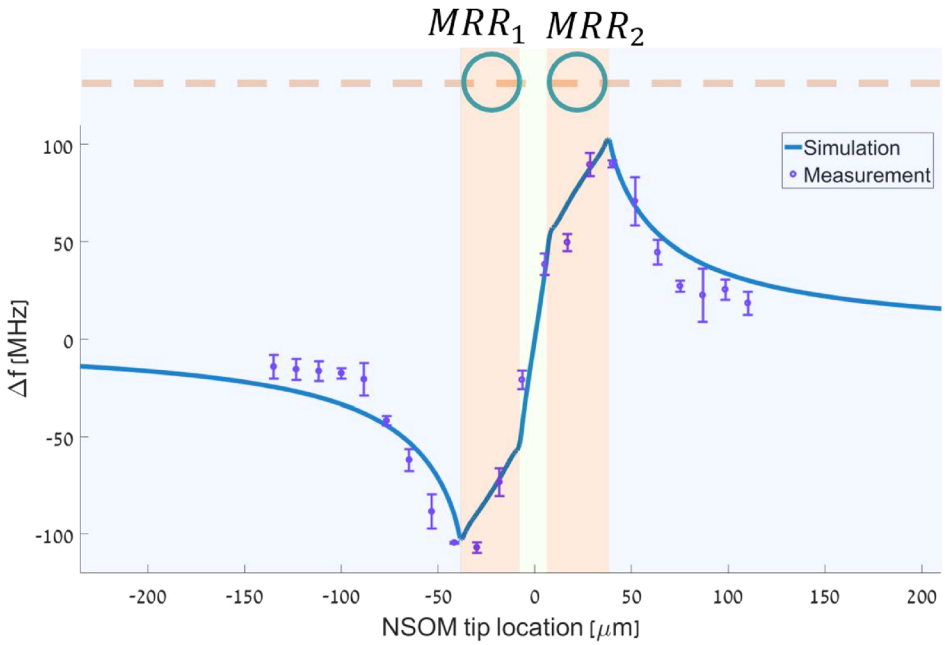

FIG. 4. Measured and simulated frequency shifts Δf due to the temperature gradient and the free carrier effect induced by the light emitting NSOM tip at different spatial positions along the line connecting the center of the MRRs, represented by an orange dashed line.

radii. As can be seen in Figs. S3 and S4 of the supplementary material, one can expect an accuracy of 50 nm for an input power of 20 μW. With a lower input power of 1 μW, the predicted accuracy reduces to $\sim$1 μm. For a relatively small beam radius, the accuracy varies very little with the beam size. As can be seen, for beam radii of 5, 15, and 30 μm, the predicted accuracies are 100,135, and 215 nm, respectively. Yet, as we further increase the beam radius, the reduction in accuracy becomes more significant. For example, a beam radius of 90 μm will result in a positioning uncertainty of about 1.4 μm. As the Allan deviation which is related to the beam positioning accuracy is inversely proportional to the Q factor,[19] a drastic improvement of position accuracy is expected if higher Q factor resonators[14] are used.

The system is operating in a common mode rejection, i.e., it only measures differential signals, and as such, it is not influenced by environmental fluctuations (temperature, humidity, pressure, etc.). The measured signal is in the radio frequency domain, which allows common and robust electrical components and measurement concepts to be integrated at low cost. As such, the demonstrated approach may serve as a cheap and simple alternative to advanced beam positioning devices.

See supplementary material for figures of the MRR resonance spectrum, Allan deviation measurements, and simulation of the effect of illumination with various beam radii and power on the resonance frequency difference between the two MRRs.

This research was supported by the Israeli Ministry of Science and Technology, and the device fabrication was made by TowerJazz FAB.

[1]G. Meyer and N. M. Amer, Appl. Phys. Lett. **53**, 1045 (1988).
[2]S. F. Tolić-Nørrelykke, Rev. Sci. Instrum. **77**, 103101 (2006).
[3]J. H. G. Huisstede, K. O. van der Werf, M. L. Bennink, and V. Subramaniam, Opt. Express **13**, 1113 (2005).
[4]R. L. Gustavson and T. E. Davis, Proc. SPIE **1633** (1992).
[5]Y. Liu, N. Xi, and Y. Shen, Int. J. Optomechatronics **5**, 170 (2011).
[6]R. Martins and E. Fortunato, Rev. Sci. Instrum. **66**, 2927 (1995).
[7]X. Zheng, S. Chen, W. Chen, X. Wu, and S. Xiang, Proc. SPIE **7514**, 75140Y (2009).
[8]M. H. Khan, H. Shen, Y. Xuan, L. Zhao, S. Xiao, D. E. Leaird, A. M. Weiner, and M. Qi, Nat. Photonics **4**, 117 (2010).
[9]J. Wang, H. Shen, L. Fan, R. Wu, B. Niu, L. T. Varghese, Y. Xuan, D. E. Leaird, X. Wang, F. Gan, A. M. Weiner, and M. Qi, Nat. Commun. **6**, 5957 (2015).
[10]Q. Xu, B. Schmidt, S. Pradhan, and M. Lipson, Nature **435**, 325 (2005).
[11]T. Baba, S. Akiyama, M. Imai, N. Hirayama, H. Takahashi, Y. Noguchi, T. Horikawa, and T. Usuki, Opt. Express **21**, 11869 (2013).
[12]H.-T. Kim and M. Yu, Opt. Express **24**, 9501 (2016).
[13]G.-D. Kim, H.-S. Lee, C.-H. Park, S.-S. Lee, B. T. Lim, H. K. Bae, and W.-G. Lee, Opt. Express **18**, 22215 (2010).
[14]A. Naiman, B. Desiatov, L. Stern, N. Mazurski, J. Shappir, and U. Levy, Opt. Lett. **40**, 1892 (2015).
[15]L. Stern, A. Naiman, G. Keinan, N. Mazurski, M. Grajower, and U. Levy, Optica **4**, 1 (2017).
[16]D. Dimitropoulos, R. Jhaveri, R. Claps, J. C. S. Woo, and B. Jalalia, Appl. Phys. Lett. **86**, 071115 (2005).
[17]A. Gajda, J. Muller, O. Nobis, J. Bruns, I. Giuntoni, M. Krause, H. Renner, K. Petermann, and E. Brinkmeyer, in *2008 5th IEEE International Conference on Group IV Photonics* (2008), pp. 173–175.
[18]R. Soref and B. Bennett, IEEE J. Quantum Electron. **23**, 123 (1987).
[19]F. Riehle, *Frequency Standards: Basics and Applications* (Wiley-Blackwell, 2005), pp. 47–79.